

# XBT data collected along the Southern Ocean “chokepoint” between New Zealand and Antarctica, 1994-2024

Giuseppe Aulicino<sup>\*,1,2</sup>, Antonino Ian Ferola<sup>1</sup>, Laura Fortunato<sup>1</sup>, Giorgio Budillon<sup>1,3</sup>, Pasquale Castagno<sup>3,4</sup>, Pierpaolo Falco<sup>3,5</sup>, Giannetta Fusco<sup>1,3</sup>, Naomi Krauzig<sup>3,5</sup>, Giancarlo Spezie<sup>1,3</sup>, Enrico Zambianchi<sup>1,3</sup>, Yuri Cotroneo<sup>\*,1,3</sup>

<sup>1</sup> Dipartimento di Scienze e Tecnologie, Università degli Studi di Napoli “Parthenope”, Napoli, 80143, Italy

<sup>2</sup> Istituto di Scienze Polari, Consiglio Nazionale delle Ricerche, Bologna, 40129, Italy

<sup>3</sup> Consorzio Nazionale Interuniversitario per le Scienze del Mare (CoNISMa), Roma, 00196, Italy

<sup>4</sup> Dipartimento di Scienze Matematiche e Informatiche, Scienze Fisiche e Scienze della Terra, Università degli Studi di Messina, 98122, Italy

<sup>5</sup> Dipartimento di Scienze della Vita e dell’Ambiente, Università Politecnica delle Marche, Ancona, 60131, Italy

\* Correspondence to: Giuseppe Aulicino (giuseppe.aulicino@uniparthenope.it); Yuri Cotroneo (yuri.cotroneo@uniparthenope.it)

**Abstract.** This study presents the water column temperature data collected during several cruises on board the *Italica*, *Araon* and *Laura Bassi* research vessels, in the framework of the Climatic Long-term Interaction for the Mass balance in Antarctica (CLIMA), Southern Ocean Chokepoints Italian Contribution (SOChIC), and Marine Observatory of the Ross Sea (MORSea) projects, funded by the Italian National Antarctic Research Program (PNRA). Data were collected between New Zealand and the Ross Sea during the austral summers from 1994/1995 to 2023/2024. Across this chokepoint of the Antarctic Circumpolar Current, XBT Sippican T7 probes were launched with a regular 20 km sampling, providing temperature profiles with a vertical resolution of 65 cm and a maximum nominal depth of 760 m. All temperature profiles underwent a rigorous quality control, including a general malfunctioning verification, the removal of spikes, the consistency check of adjacent profiles, the comparison to regional oceanographic features and satellite altimetry observations, and a final visual check by operator. Data quality checks led us to discard about 12% of acquired XBT measurements. This dataset contributes to the improvement of our understanding of Southern Ocean features, being highly valuable for studies focusing on climate variability, especially across the Antarctic Circumpolar Current and its fronts. Furthermore, we expect that the collected XBT data will serve as a useful tool for the calibration and validation of recent satellite observations and for the improvement of Southern Ocean oceanographic simulations.

## 1 Introduction

The temperature of the ocean is one of the key parameters identified by the Global Climate Observing System (GCOS) as being essential for climate studies (World Meteorological Organization, 2016). Together with salinity values, ocean temperatures are necessary to identify and trace the main water masses and monitor their evolution at different spatial and temporal scales.

On the larger scales, collecting oceanic temperature and salinity data is of paramount importance to the study of the global thermohaline circulation, which plays a pivotal role in Earth's climate system. The Southern Ocean (SO) plays a fundamental role in this circulation (Gille, 1994; Rintoul, 2018), as some of the global thermohaline circulation "engines" are located near the Antarctic coast, associated with polynya areas (Morales Maqueda et al., 2004; Aulicino & Wadhams, 2022). At smaller scales, temperature data can be used to describe the vertical structure of the ocean (e.g., the thermocline depth and its variability), to locate fronts between different water masses, determine the ocean heat content and volume transport, and to identify meso- and sub-mesoscale ocean dynamics. The main current in the SO is the Antarctic Circumpolar Current (ACC), which is its primary source of heat, nutrients and momentum (Sokolov & Rintoul, 2009a, 2009b). The ACC is one of the largest currents on the planet, flowing from west to east and isolating the Antarctic continent, which makes it strongly dependent on the SO conditions. Additionally, the Antarctic ecosystem is very fragile and temperature-dependent, which highlights the importance of monitoring physical changes in the ocean that surrounds it (Convey & Peck, 2019). Therefore, monitoring the SO and its temperature is essential for improving our knowledge of the processes driving the Antarctic variability and the global climate balance (Rintoul, 2018; Armour et al., 2016).

Despite its importance, SO has consistently faced a scarcity of in situ observations due to its remote location and the extreme weather conditions, which often hinder research activities to be carried out on site. The measurements are further limited by the seasonal sea ice presence that inhibits the navigation and the data collection. Additionally, in situ data collection is often conducted with instruments and probes used from ships travelling at their normal speed (e.g., Expendable BathyThermographs – XBT), without the possibility to perform classical full depth CTD casts that require ship stops. The advent of the international ARGO program increased significantly the number of hydrographic observations available in the SO throughout all seasons (Roemmich et al., 2022). However, Lagrangian floats do not allow the collection of information along repeated monitoring lines.

Accordingly, many steps have been taken over time to obtain ocean temperature data through remote sensing. Satellite data provide valuable insights about the upper ocean, especially when considering that the surface layer is closely related to fundamental phenomena (e.g., ocean-atmosphere physical

70 and biogeochemical interactions, fronts, currents, meanders, eddies) impacting the large-scale  
71 circulation and the meso- and small-scale characteristics of the ocean (e.g., McGillicuddy, 2016;  
72 Cotroneo et al., 2016; Seo et al., 2023). Additional information about the water column can also be  
73 retrieved from numerical models (e.g., Downes et al., 2015) and 3D reconstructions inferred through  
74 machine learning and statistical techniques applied to satellite observations, such as sea surface  
75 temperature (e.g., Buongiorno Nardelli et al., 2020). Nonetheless, in situ measurements are  
76 indispensable for achieving the necessary precision and depth coverage. In addition, they provide  
77 critical ground-truth for the calibration and validation of satellite retrievals of surface variables, and  
78 the improvement of data acquisition algorithms (Aulicino et al., 2022). It is therefore evident that the  
79 collection of in situ data is essential for monitoring ocean temperature.

80 The Global Ocean Observing System (GOOS) Ship Of Opportunity Program (SOOP), and the related  
81 Ship of Opportunity Program Implementation Panel (SOOPIP), address scientific and operational  
82 (standardization, maintenance, and advancement of the instruments and techniques) goals,  
83 respectively, to building a sustained ocean observing system, e.g., supplementing dedicated research  
84 vessels in the collection of upper ocean in situ XBT data through the use of ships that are already  
85 traversing the world's oceans (Legler et al., 2015; Goni et al., 2019).

86 In this scenario, the University of Naples Parthenope has been taking part since 1994 in the  
87 organization and execution of several oceanographic campaigns along the PX36 monitoring line in  
88 the Pacific sector of the SO, i.e., between New Zealand and the Ross Sea, in the framework of the  
89 Italian National Antarctic Research Program (PNRA). During each expedition, XBT launches were  
90 carried out, collecting ocean temperature data from surface to a maximum of about 760m depth (Falco  
91 et al., 2022). This study presents the collected XBT dataset, which significantly contributes to the  
92 accessibility of extensive ocean temperature data.

93 In this paper, the methodologies used for data collection and quality control (QC) are described in  
94 Section 2; the results and the discussion are reported in Section 3; the data record details and the  
95 conclusions are summarized in Section 4.

96

## 2 Data and methods

### 2.1 The XBT dataset

An XBT system is composed of several key components: an expendable ballistic probe that descends into seawater; a data acquisition device that records an electrical signal and converts it into usable numerical data (with the support of a computer unit); a double copper wire that connects the falling probe to the acquisition device (Goni et al., 2019; Parks et al., 2022; Simoncelli et al., 2024). As the probe descends through the water column, temperature measurements are acquired using a Negative Temperature Coefficient (NTC) thermistor mounted on the probe zinc nose, which alters its resistance in response to the seawater temperature it comes into contact with. The insulated copper wire is unwound simultaneously by two spools, i.e., clockwise on the ship and counterclockwise in the falling probe. This technique decouples the XBT vertical descent through the seawater from the ship translational motion (Simoncelli et al., 2024). Data recording continues until the wire breaks or the recording is terminated by the operator. The depth associated with a temperature measurement is not sensed directly because XBT probes do not contain pressure sensors. Instead, it is estimated using a phenomenological Fall Rate Equation (FRE) provided by the manufacturer, with coefficients that vary based on the probe type and year. These coefficients, along with details about the data acquisition systems, are typically included in the metadata associated with each XBT cast.

The uncertainties on temperature and pressure values make the XBT probe accuracy be generally rated to  $\pm 0.10^{\circ}\text{C}$  (Parks et al., 2022), although differences can be retrieved depending on the manufacturer and the manufacturing date of different devices (Cowley et al., 2013). Consequently, some crucial information should be always provided with any XBT dataset for subsequent optimal use of the measurements, including a complete description of the system characteristics in the metadata (e.g., probe type, fall rate coefficients, data originator, platform).

We present here the dataset of water column temperatures collected in the Pacific sector of the Southern Ocean through XBT casts during several research cruises on board the Italian research vessels “Italica” and “Laura Bassi” and the Korean icebreaker “Araon” (see Table 1). These activities were carried out in the framework of the Italian PNRA by several scientific projects, e.g., Climatic Long-term Interaction for the Mass balance in Antarctica (CLIMA), Southern Ocean observing system and Chokepoints Italian Contribution (SOChIC) and Marine Observatory in the Ross Sea (MORSea).

The XBT casts were carried out during the austral summers between 1994/1995 and 2023/2024, mainly in January and February (Figure 1), using Sippican T7 probes providing temperature profiles with a vertical resolution of 65 cm and a maximum nominal depth of 760 m. Only during the 1994/1995 (PNRA\_X) and 1995/1996 (PNRA\_XI) cruises some Sippican T5 probes were used,

reaching a maximum depth of 1830 m, as reported in the campaign metadata information (Table 2). The majority of transects were completed in 5-6 days and provide a synoptic picture of the thermal structure of the upper SO across its Pacific Sector (Figure 2). A regular 20 km sampling interval was adopted with occasional increased sampling frequency over the main frontal regions of the ACC.

135

**Table 1.** List of scientific cruises included in this dataset carried out between November 1994 and January 2024

Cruise name	R/V	Start date	End date	Latitude	Longitude
PNRA_X	ITALICA	03 November 1994	02 March 1995	47.00 - 74.99°S	172.02°E - 175.90°W
PNRA_XI	ITALICA	07 January 1996	18 February 1996	48.66 - 72.01°S	173.56°E - 179.79°E
PNRA_XII	ITALICA	26 January 1997	19 February 1997	46.17 - 74.69°S	166.24°E - 179.82°E
PNRA_XIII	ITALICA	23 November 1997	06 March 1998	46.25 - 72.71°S	171.39°E - 179.43°W
PNRA_XIV	ITALICA	05 January 1999	11 January 1999	48.07 - 69.00°S	173.70°E - 178.55°E
PNRA_XV	ITALICA	07 January 2000	18 February 2000	49.17 - 69.83°S	173.13°E - 178.41°E
PNRA_XVI	ITALICA	06 January 2001	26 February 2001	48.75 - 75.94°S	170.59°E - 179.72°E
PNRA_XVII	ITALICA	24 December 2001	31 December 2001	48.50 - 69.30°S	160.39°E - 178.01°E
PNRA_XVIII	ITALICA	06 January 2003	11 January 2003	48.00 - 71.26°S	172.93°E - 177.47°E
PNRA_XIX	ITALICA	24 December 2003	28 December 2003	46.36 - 66.17°S	173.81°E - 179.99°E
PNRA_XX	ITALICA	01 January 2005	06 January 2005	48.03 - 70.49°S	174.22°E - 178.38°E
PNRA_XXI	ITALICA	01 January 2006	04 January 2006	48.03 - 66.50°S	174.59°E - 179.93°E
PNRA_XXII	ITALICA	05 February 2007	10 February 2007	47.23 - 71.99°S	170.86°E - 174.26°E
PNRA_XXIII	ITALICA	16 January 2008	21 January 2008	47.50 - 68.99°S	174.18°E - 178.63°E
PNRA_XXV	ITALICA	25 January 2010	29 January 2010	46.38 - 70.00°S	173.63°E - 178.00°E
PNRA_XXVII	ITALICA	13 January 2012	19 January 2012	47.85 - 65.96°S	172.03°E - 176.54°E
PNRA_XXVIII	ARAON	24 January 2013	06 February 2013	47.20 - 68.5°S	158.30°E - 177.00°E
PNRA_XXIX	ITALICA	30 December 2013	18 February 2014	48.01 - 78.83°S	167.07°E - 175.84°W
PNRA_XXX	ARAON	02 January 2015	10 January 2015	47.99 - 73.22°S	157.02°E - 173.81°E
PNRA_XXXI	ITALICA	16 January 2016	28 January 2016	47.49 - 72.40°S	171.56°E - 175.00°E
PNRA_XXXII	ITALICA	31 December 2016	05 January 2017	48.01 - 68.77°S	174.09°E - 179.85°W
PNRA_XXXIV	ARAON	08 February 2019	12 February 2019	47.99 - 69.75°S	166.79°E - 170.87°E
PNRA_XXXV	LAURA BASSI	07 January 2020	12 January 2020	48.01 - 69.25°S	172.97°E - 178.84°E
PNRA_XXXVI	LAURA BASSI	25 December 2020	02 January 2021	46.96 - 73.39°S	172.82°E - 175.89°E
PNRA_XXXVII	LAURA BASSI	08 January 2022	26 January 2022	47.54 - 76.35°S	171.20°E - 177.58°W
PNRA_XXXVIII	LAURA BASSI	06 January 2023	12 January 2023	46.56 - 72.27°S	169.40°E - 178.70°E
PNRA_XXXIX	LAURA BASSI	07 January 2024	12 January 2024	48.20 - 70.00 °S	166.30 °E – 176.40°E

137

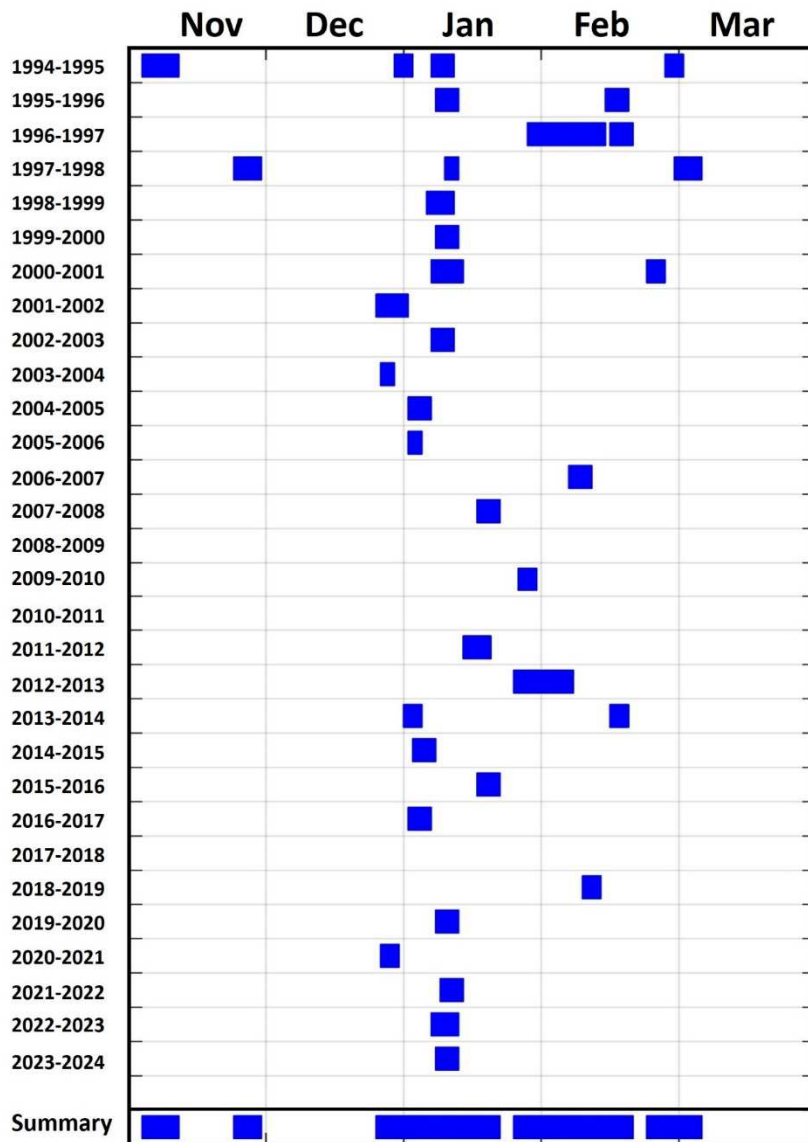
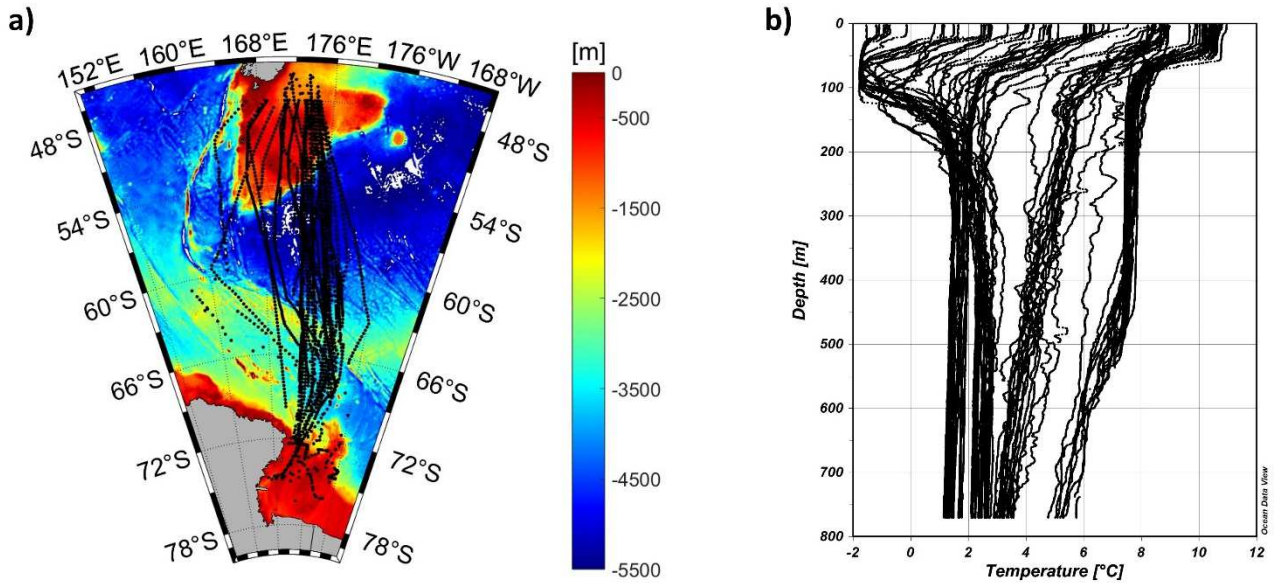


**Figure 1.** Temporal distribution of the oceanographic campaigns conducted along the New Zealand-Antarctica “chokepoint” between 1994 and 2024.

**Table 2.** Characteristics of the different XBT probes used in this study: nominal depth guaranteed by Sippican; maximum ship speed suggested by Sippican for an optimal drop; amount of ZAMAK (a zinc-based alloy enriched with aluminium, magnesium, and copper), copper and plastic for each probe type (adapted from Simoncelli et al., 2024)

Probe type	Max rated depth (m)	Max ship speed (knots)	ZAMAK (kg)	Plastic (kg)	Copper (kg)
Sippican T5	1830	6	0.613	0.125	0.357
Sippican T7	760	15	0.576	0.052	0.240



151

152 **Figure 2. a)** Map of the Southern Ocean area between New Zealand and Antarctica. The black dots represent the position  
 153 of all XBT launches carried out between December 1994 and January 2024. **b)** An example of temperature vertical profiles  
 154 collected through XBT across the New Zealand – Ross Sea chokepoint during the XXXV Italian Antarctic Expedition.

155

156

157

## 2.2 Quality Control

158 Various types of malfunctions can affect XBT measurements and result in inaccurate temperature  
 159 readings within the temperature profile. These faults can appear as a spike in a single recorded value  
 160 or affect the temperature across a range of depths. Moreover, some issues can create errors that mimic  
 161 real phenomena, such as temperature inversions or fronts (Parks et al., 2022; Cowley and Krummel,  
 162 2022). Sometimes, profiles can be corrected by deleting or filtering sections of the original data.  
 163 However, an accurate quality control procedure must be implemented before any data is discarded or  
 164 manipulated. Additionally, a flagging scheme is generally applied to provide XBT dataset users with  
 165 quality indicators of the oceanographic data.

166 Quality flags (QFs) are essential for enabling users to filter the XBT dataset according to the specific  
 167 quality requirements for the intended use. Several flagging scheme exist in agreement with  
 168 recommendations provided by the Intergovernmental Oceanographic Commission of UNESCO  
 169 (IOC, 2013). In this study we follow the suggestions provided by the Global Temperature and Salinity  
 170 Profile Program (GTSP) of the NOAA-NCEI (<https://www.ncei.noaa.gov/products/global-temperature-and-salinity-profile-programme>) resulting in the flagging scheme summarized in Table  
 171 3 for indicating the quality of each temperature and depth data point.  
 172

173

174 **Table 3.** The Quality Flags (QF) assigned to the XBT data

QF	Quality	Description
0	No QC	No quality control has been performed on this data.
1	Good data	The data is good. No malfunctions have been identified and consistency with real phenomena has been verified.
2	Probably good data	Minor malfunctions present which are small or correctable without affecting overall data quality. Some features (probably real) are present but these are unconfirmed.
3	Probably bad data	Data are suspect and present unusual features which are inconsistent with real phenomena, Data remains potentially correctable.
4	Bad data	The data appears erroneous. Evident errors are identified and there is no likelihood of correction.

175

176

177 The assignment of QFs is the result of a series of quality control (QC) tests for both temperature and  
178 depth data which are used to get a reliable quality check of the temperature measurements collected  
179 through our XBTs and of the retrieved depths. Results of each test allowed to insert the relative flag  
180 to the corresponding measurement according to the scheme shown in Table 3. QF=1 is assigned when  
181 all the tests pass and QF=4 when at least one test fails. For temperature, more detailed checks are  
182 performed, including a final visual check, allowing us to introduce QF=2 and QF=3 for probably  
183 good and probably bad data, respectively (as detailed below).

184 Overall, the QC procedures applied to our dataset follow recommendations previously suggested by  
185 NOAA, developed and refined in the last three decades (Bailey et al., 1994; Daneshzadeh et al., 1995;  
186 Cowley and Krummel, 2022; Parks et al., 2022; Tan et al., 2023). These procedures include several  
187 steps undertaken in a top-down manner, as temperature data are measured from the surface down,  
188 and faults that occur at a given depth may impact on deeper data (Parks et al., 2022).

189 First, each XBT profile was tested for invalid metadata information, such as the correct time, cast  
190 position and any other possible operator errors, using a sequence of independent checks. All identified  
191 errors in date and time were corrected accordingly, with the support of the XBT launch log sheets  
192 provided by operators on board. No errors were found concerning the position of the casts after the  
193 comparison of latitudes and longitudes against gridded GEBCO 2 x 2 minutes bathymetry (GEBCO  
194 Compilation Group, 2023). The check of unrealistic positions was also performed using the  
195 calculation of vessel speed from profile date and time and an upper general threshold of 20 knots  
196 (since most of the launches are realized by ships travelling in the range of 10/15 knots). Additionally,  
197 the depth values of each XBT profile were compared to the last good depth value provided by the  
198 operators (QF=1 is assigned to shallower depth values, otherwise they are flagged as QF=4).



Then, all the vertical temperature profiles were checked for nominal maximum depth (760 m), and carefully inspected to identify malfunctions, coherence to regional oceanographic features, drop-to-drop consistency along the cruise track, and presence of unusual features. In this context, the main difficulty is usually found in distinguishing a common malfunction from a regional oceanographic feature (i.e., unexpected increase of temperature southward or along the water column). Consequently, unusual features were cross-validated by comparison to repeated (within 15 minutes) or neighbouring profiles from the same voyage and eventually to available Austral summer ARGO observations over the study area. To this aim, we took again advantage of XBT launch log sheets, in which operators notified any instrument malfunctions, adverse weather conditions, sea ice presence and local bottom depth. In particular, the bottom depth was relevant to constraining XBT data profiles at the right depth, especially when approaching shallow waters (QF=1 is assigned to values shallower than bottom depth, otherwise they are flagged as QF=4). When the log sheet was unavailable, we relied instead on the GEBCO 2 x 2 minutes bathymetry (GEBCO et al., 2023), which closely corresponded to the in situ reported depths over the area and period of study. Additionally, a gross filter was applied to all the XBT profiles using temperature ranges that vary on four vertical layers, as reported in Table 4. The ranges were defined through the use of ARGO data collected in the study area between 2004 and 2023. QF=4 was applied to data exceeding the thresholds of  $\pm 0.5^{\circ}\text{C}$ .

**Table 4.** Temperature ranges applied to XBT profiles, defined in four levels.

Depth range (m)	Temperature minimum ( $^{\circ}\text{C}$ )	Temperature maximum ( $^{\circ}\text{C}$ )
0 - 100	-1.866	14.698
100 - 250	-1.865	11.093
250 - 500	0.068	8.717
500 - 760	0.826	8.266

Several studies assess that the XBT measurements near the sea surface may be considered unreliable due to the stabilization of motion and thermal adaptation to the surrounding environment (e.g. Bailey et al., 1994; Cowley and Krummel, 2022; Simoncelli et al., 2024). They also suggest that the first acceptable value is at about 4 m depth and that the data user must be carefully informed in order to exclude suspect surface values from scientific analyses. Here, we opted for providing all the original measurements annotating their quality, as resulting from a dedicated test on the initial part of each profile. This test calculates the differences between the value recorded at time  $t = 0.6$  s (about 4 m depth) and shallower measurements, classifying them based on the standard uncertainty on

228 temperature attributable to an XBT probe (0.10 °C) as a metric (Simoncelli et al., 2024). Therefore,  
229 temperature data are assigned QF=1 if the difference is less than or equal to standard deviation (std);  
230 QF=2 if it is comprised between std and 2\*std; QF=3 if it is comprised between 2\*std and 3\*std; and  
231 QF=4 if it is higher than 3\*std.

232 Then, the XBT profiles were examined for the presence of spikes, unrealistic oscillations and unusual  
233 gradients in temperature data, as well as sharp variations toward negative or higher values, which  
234 could be caused by copper wire breaks. Data are mostly flagged as good (QF=1) or bad (QF=4)  
235 values. Nonetheless, suspect data are compared with neighbouring profiles and ARGO climatology  
236 over the study area (obtained from products available at [https://www.coriolis.eu.org/Data-](https://www.coriolis.eu.org/Data-Products/Data-selection)  
237 [Products/Data-selection](https://www.coriolis.eu.org/Data-Products/Data-selection)), eventually assigning QF=1, QF=2 and QF=3 attributes. For example, QF=2  
238 is used when an XBT profile presents a step-like feature that is not confirmed by a neighbouring  
239 profile but is consistent with similar features previously observed in the study region. QF=3 is used,  
240 instead, when XBT values exhibit suspect temperature values that cannot be confirmed by a  
241 neighbouring profile and occur in areas where there is no evidence of mesoscale structures (e.g.,  
242 eddies or fronts).

243 Nevertheless, an increase or decrease in temperature over large depth ranges compared to  
244 neighbouring profiles, can be also associated to an eddy, a frontal area or an intense current system.  
245 Therefore, QF=1 is applied when repeated profiles showing similar temperatures or archive data can  
246 confirm the feature. The larger scale description of ocean dynamics obtained through satellite  
247 altimetry was also used for controversial results to identify the presence of eddies and frontal systems  
248 affecting the temperature data.

249 However, some profiles might exhibit anomalous features that the described QC procedure could not  
250 detect as erroneous values. Therefore, an additional visual check was carried out for each individual  
251 cruise track and each vertical temperature profile to verify the assigned QF=2 and QF=3 flags and  
252 identify any residual anomalies in the positioning of the XBT launches or outliers in the data  
253 collection. This control was performed using the Ocean Data View (ODV) software (Schlitzer, 2023).  
254 Overall, the entire QC led us to discard about 12% of acquired XBT observations, which were flagged  
255 as bad or probably bad data (Figure 3).

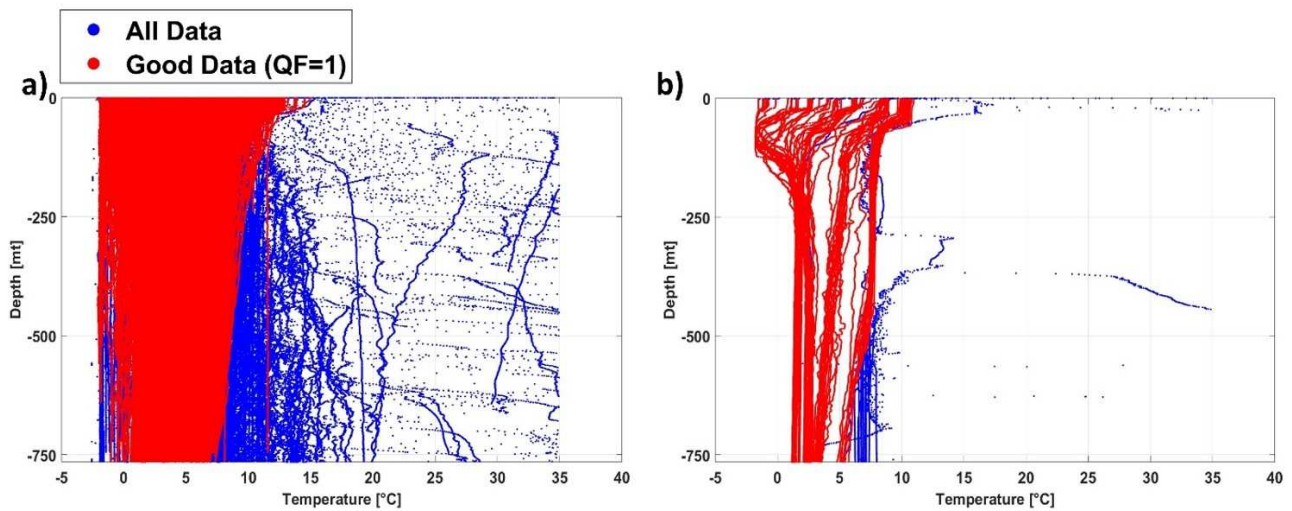


**Figure 3. a)** XBT observations collected between December 1994 and January 2024 over the New Zealand – Ross Sea chokepoint before (blue) and after (red) the quality check; **b)** An example of the quality check on the XBT data collected during the PNRA\_XXXV cruise.

### 2.3 XBT data biases correction

Previous studies assessed that temperature biases and depth errors, due to inaccurate time conversion to depth through FRE, may affect XBT observations (e.g., Gouretski and Reseghetti, 2010; Cowley et al., 2013). Although a full comprehension of the origins of these issues is still pending, several experiments tried to quantify this bias by comparing XBT profiles with co-located CTD observations, demonstrating that XBT temperatures are usually warmer than reality (Gouretski and Reseghetti 2010; Cheng et al., 2014). Different possible causes of biases emerged, including mechanical (e.g., probe type, manufacturer, year), external (e.g., launch height, meteo-marine conditions) and electrical (e.g., thermistor, wire) factors (Seaver and Kuleshov 1982; Green, 1984; Reverdin et al. 2009). Additionally, a decrease in fall rate was observed in cooler waters because of increased viscosity (Gouretski and Reseghetti 2010), making FRE corrections in the Southern Ocean extremely important (Cheng et al., 2014).

To address these problems, several correction schemes have been proposed over the past few decades. A comprehensive list of related papers is available at <https://www.ncei.noaa.gov/products/xbt-corrections>. Taking advantage of more than 220,000 XBT-CTD side-by-side pairs, Cheng et al. (2014) examined and compared existing methodologies, proposing a new correction scheme for historical XBT data for nine independent probe-type groups. Their study confirmed that depth error and pure temperature bias are temperature-dependent and may be influenced by the data acquisition and recording system. Moreover, the resulting scheme also considers that some biases affecting the

281 XBT-derived temperature profiles vary with manufacturer/probe type and have been shown to be  
282 time dependent, and that depth correction varies with depth (Cheng et al. 2016).  
283 In our dataset, we apply this methodology, which includes corrections for both temperature and depth  
284 values based on calendar year, water temperature, and probe type, to provide bias-corrected XBT  
285 measurements (Cheng et al., 2014). To this aim, we use the Hanawa et al. (1995) coefficients (i.e.,  
286  $A=6.691$ ,  $B=0.00225$ ) in the Fall Rate Equation  $D(t) = At - Bt^2$  to derive temperature measurement  
287 depths starting from the time elapsed since the probe's release and, consequently, the bias-corrected  
288 depth and temperature values. A full description of the methodology is available at  
289 <https://www.ncei.noaa.gov/products/xbt-corrections> (see CH Correction Method); the update tables  
290 of the applied coefficients are available at  
291 [http://www.ocean.iap.ac.cn/ftp/images\\_files/CH14\\_description/CH14\\_table1\\_update2023.txt](http://www.ocean.iap.ac.cn/ftp/images_files/CH14_description/CH14_table1_update2023.txt) and  
292 [http://www.ocean.iap.ac.cn/ftp/images\\_files/CH14\\_description/CH14\\_table2\\_update2023.txt](http://www.ocean.iap.ac.cn/ftp/images_files/CH14_description/CH14_table2_update2023.txt).

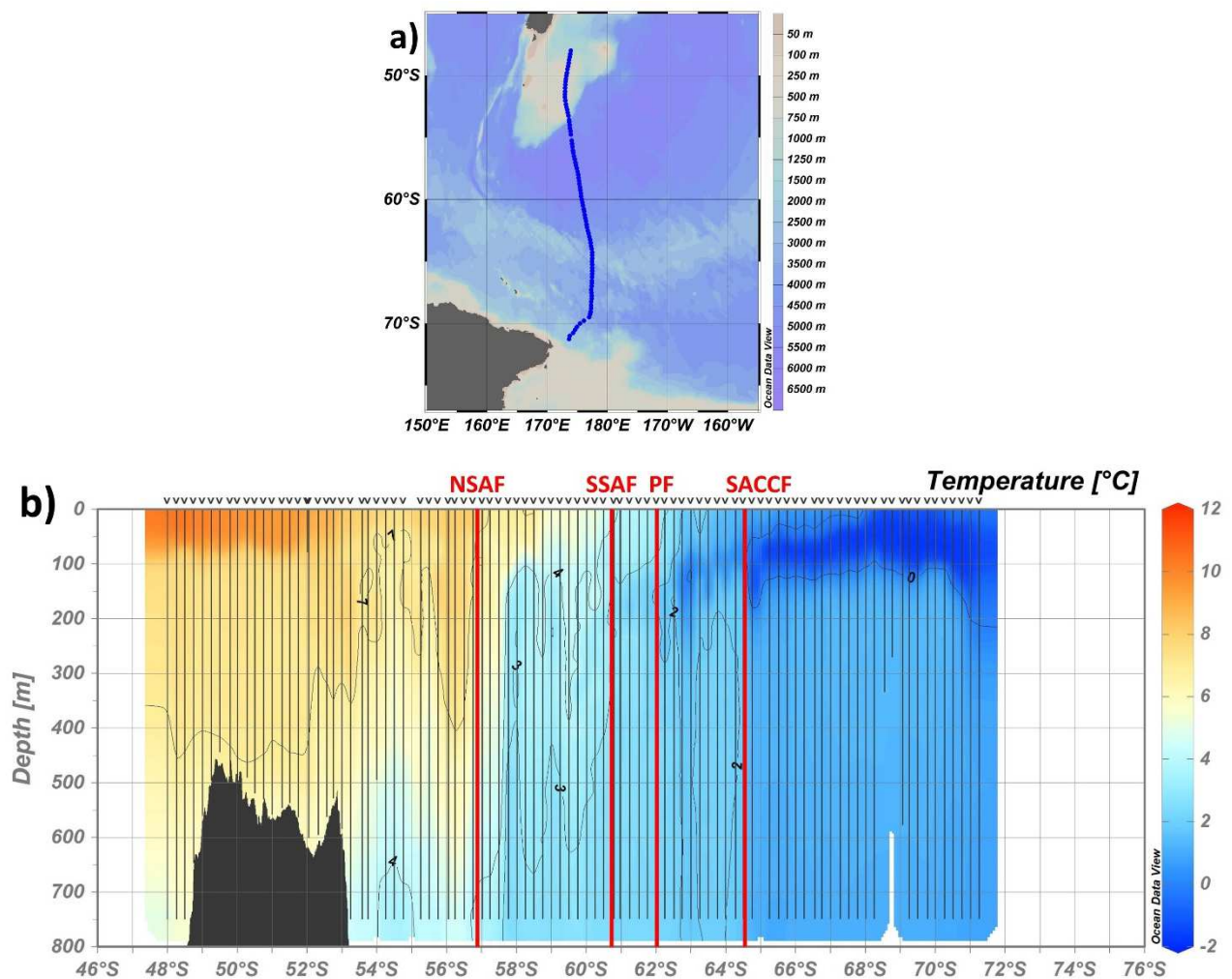
### 295 **3. Results and discussion**

296 We believe this exceptional temperature dataset provides a valuable reservoir of high-resolution,  
297 independent, and trustworthy information. The dataset assumes notable significance, representing an  
298 extensive temporal series of data collected nearly every austral summer over the last 30 years, within  
299 the same oceanic sector of the SO and along the same monitoring transect (PX36). We exploited this  
300 information to provide 36 vertical sections of the ocean temperature, from the surface to about 800 m  
301 depth, along the New Zealand–Antarctica “chokepoint”. Figures representing the latitudinal sections  
302 of corrected XBT temperatures during each leg are available in the supplementary information  
303 (Figures S1-S36). All the temperature sections presented in Figures 4, 6, and S1-S36, were realized  
304 using ODV software and applying consistent interpolation parameters. The adopted zonal  
305 interpolation is based on a spatial weighting model that incorporates three temperature profiles (a  
306 central reference profile, an upstream profile, and a downstream profile), considering a maximum  
307 influence range of 60 km along the zonal direction and 20 m along depth.

308 The repeated temperature sections significantly enhance our understanding of ACC fronts and their  
309 evolution over the last three decades. A first application of the dataset is shown in Figure 4 where  
310 XBT observations collected during the PNRA\_XVIII expedition are used for the identification of the  
311 main ACC fronts positions: Northern Sub Antarctic Front (NSAF); Southern Sub Antarctic Front  
312 (SSAF); Polar Front (PF); Southern Antarctic Circumpolar Current (sACCF). The criteria used for  
313 identifying the fronts (Table 5) follow Budillon and Rintoul (2003), which compiles several  
314 hydrographic definitions (Botnikov, 1963; Belkin, 1990; Orsi et al., 1995; Rintoul et al., 1997). The

315 Southern boundary of the ACC, usually described as the maximum southern extent of vertical  
 316 maximum of  $T > 1.5^{\circ}\text{C}$  at about 200 m (Orsi et al., 1995), is not described in this sector as its position  
 317 is coincident with the sACCf position in most of the available temperature sections.  
 318 The ACC fronts positions retrieved through XBT data also serve as ground truth for the validation of  
 319 those retrieved through satellite altimetry (e.g., Sokolov and Rintoul 2009a, 2009b; Graham et al.,  
 320 2012; Chapman, 2017), thereby enhancing the identification process of fronts within the SO. This is  
 321 highly desirable in regions significantly influenced by topographic steering, such as the area south of  
 322 New Zealand, where the presence of the Campbell Plateau strongly affects the ACC path (Figure 5).  
 323  
 324

325



326

327 **Figure 4.** a) Map of the position (blue dots) of all XBT launches carried out during the PNRA\_XVIII expedition along  
 328 the New Zealand–Antarctica “chokepoint” (6-11 January 2003). b) Temperature vertical section from XBT data in a) in  
 329 which the vertical black lines represent the XBT casts and the red ones the ACC main fronts positions: Northern Sub  
 330 Antarctic Front (NSAF); Southern Sub Antarctic Front (SSAF); Polar Front (PF); Southern Antarctic Circumpolar Front  
 331 (SACCf). The black mask represents the bathymetry. Figures are produced through Ocean Data View.

332

333 **Table 5.** Criteria for front definitions (Adapted from Budillon & Rintoul, 2003)

Front	Definition	Reference
Southern Antarctic Circumpolar Current Front (sACCF)	$T > 1.8^{\circ}\text{C}$ along the $T_{\text{max}}$ at depth $> 500$ m, farther north; $T < 0^{\circ}\text{C}$ along the $T_{\text{min}}$ at depth $< 150$ m, farther south.	Orsi <i>et al.</i> 1995.
Polar Front (PF)	$T < 2^{\circ}\text{C}$ at 200 m, farther south.	Botnikov 1963, Orsi <i>et al.</i> 1995.
Subantarctic Front (SAF)	Maximum temperature gradient in the range $3\text{--}8^{\circ}\text{C}$ at 300 m.	Belkin 1990.
Northern Sub-Antarctic Front (NSAF)	Maximum temperature gradient in the range $4\text{--}7^{\circ}\text{C}$ at 300 m.	Rintoul <i>et al.</i> 1997.
Southern Sub-Antarctic Front (SSAF)	Maximum temperature gradient in the range $3\text{--}4^{\circ}\text{C}$ at 300 m.	Rintoul <i>et al.</i> 1997.

334

335

336 To point out differences and similarities between ACC fronts positions identified through XBT and  
 337 satellite observations, in Figure 5 we present a Sea Surface Height (SSH) map of the study area,  
 338 averaged over the period covered by the temperature section in Figure 4 (about 7 days). To identify  
 339 the ACC fronts from satellite data, we applied the SSH isolines methodology that associates a specific  
 340 value of SSH with each front. For the selection of these values, we relied on previous studies (Sokolov  
 341 and Rintoul 2007, 2009a, 2009b) proving that the multiple jets of ACC fronts are consistently aligned  
 342 with streamlines identified by nearly constant circumpolar values of SSH contours.

343 Furthermore, ACC fronts exhibit instabilities that give rise to the generation of eddies.  
 344 Eddies, characterized as vortices pervading the ocean, assume a pivotal role, particularly within the  
 345 SO, contributing significantly to the transfer of heat, nutrients, and momentum (e.g., Chelton et al.  
 346 2011a; Falco and Zambianchi, 2011; Cotroneo et al., 2013; Trani et al., 2014; Rintoul, 2018; Menna  
 347 et al., 2020). While altimetry proves valuable in gaining insights into surface eddy dynamics, it cannot  
 348 provide information regarding vertical temperature variations within the eddy structure. Through the  
 349 temperature sections derived from XBT data, we can discern the presence or absence of an eddy and  
 350 get basic observations for the analysis of its heat content.

351 An example is provided in Figure 6 where we present the latitudinal section of temperatures observed  
 352 during the return leg of the 2013-2014 Italian Antarctic expedition (PNRA\_XXIX). This section  
 353 shows the intrusion of a cold core eddy at about  $53^{\circ}\text{S}$ , next to the Campbell Plateau edge. The eddy  
 354 is characterized by a maximum negative temperature anomaly (eddy's core) of about  $-4^{\circ}\text{C}$  compared  
 355 to the surrounding water. This negative anomaly results in the formation of a depression in the SSH,  
 356 also detectable in satellite imagery. In the SSH map shown in Figure 7, the cold core eddy is identified  
 357 as a closed circle of the blue isoline associated with the SSAF.

358

359



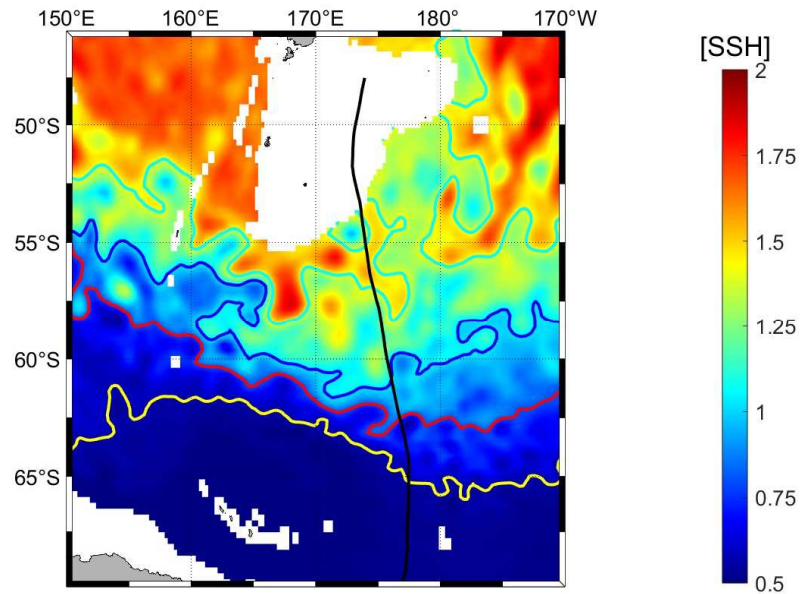
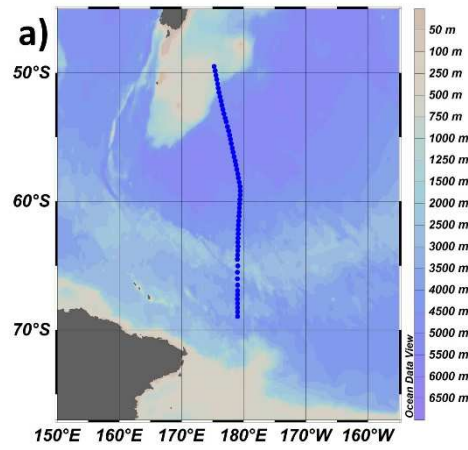


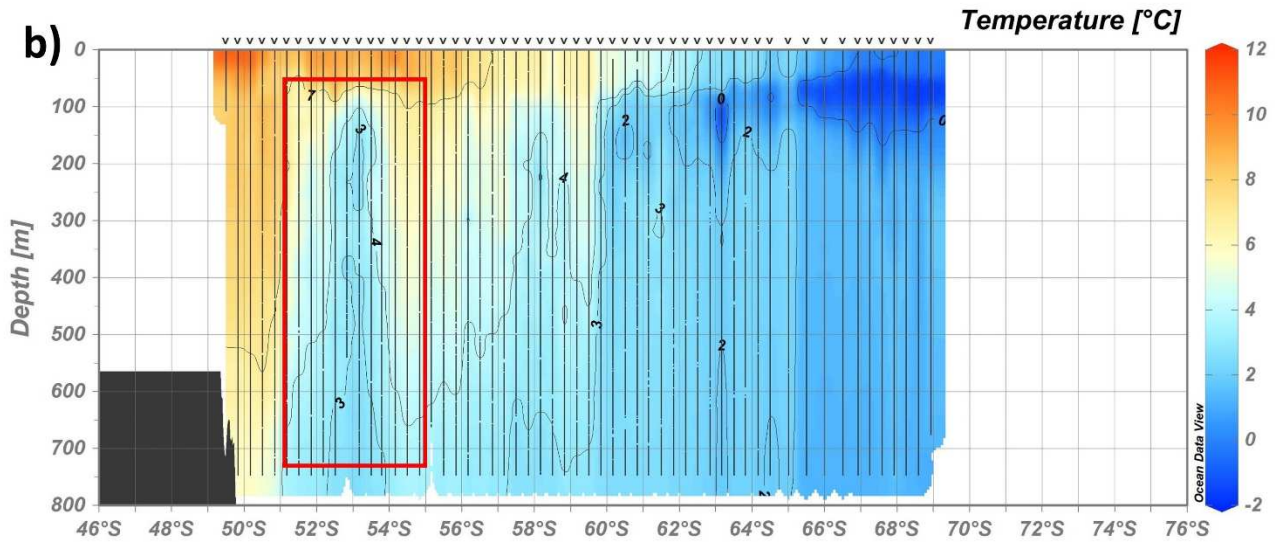
**Figure 5.** Altimetric map of SSH mediated throughout the PNRA\_XVIII expedition along the PX36 monitoring line. Contours of different colours identify the position of the main fronts of the ACC retrieved through SSH: NSAF in cyan; SSAF in blue; PF in red and sACCf in yellow. White crosses represent the position of the fronts derived from XBT data. The ship's route is represented by the black line.

Generally, the combined use of in situ observations and satellite data is crucial as it prevents errors in front positioning and eddy identification. Strong horizontal temperature gradients, often linked to eddies, could be misinterpreted as ACC fronts. Similarly, this approach allows us to distinguish eddies from other mesoscale structures, a difficult task when relying only on altimetry. XBT and satellite information are also complementary in providing valid terms of comparison, at different temporal and spatial scales (XBT at fine-scale; altimetry at meso- and large-scale), for numerical model products representing ocean circulation and eddies dynamics (e.g., Chen X. et al., 2024; Chen Z. et al., 2024).

376



377



378 **Figure 6. a)** Map of the position (blue dots) of all XBT launches carried out during the PNRA\_XXIX expedition along  
 379 the New Zealand–Antarctica “chokepoint” (30 December 2013 – 18 February 2014). **b)** Temperature vertical section  
 380 from XBT data in a) in which the vertical black lines represent the XBT casts and the red box identifies the position of  
 381 an ACC’s cold core eddy. The black mask represents the bathymetry. Figures are produced through Ocean Data View.

382



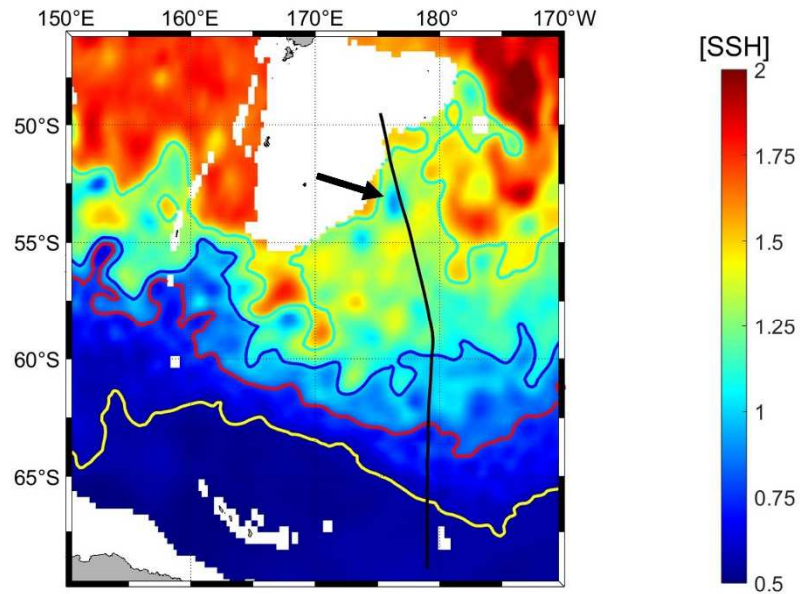


**Figure 7.** Altimetric map of SSH mediated throughout the PNRA\_XXIX expedition along the PX36 monitoring line. Contours of different colours identify the position of the main fronts of the ACC retrieved through SSH: NSAF in cyan; SSAF in blue; PF in red and sACCf in yellow. White crosses represent the position of the fronts derived from XBT data. The ship's route is represented by the black line. The black arrow indicates the observed cold core eddy.

#### 4. Data availability

The full XBT dataset presented here is publicly accessible as text format files at <https://doi.org/10.5281/zenodo.14848849>. Individual cruise data files are also available through the National Oceanic and Atmospheric Administration (NOAA) National Centers for Environmental Information (NCEI) unrestricted repositories, as listed in Table 6. NCEI serves as the official archive for data, metadata, and products collected and provided by NOAA scientists. Additionally, NCEI hosts quality checked data from non-NOAA scientists, which must go through a scientific appraisal process before being accepted into the archive. For this reason, our XBT data underwent a thorough review and improvement process (see sections 2.2 and 2.3) prior to publication, resulting in the version-3 products. Nevertheless, as noted above, the full dataset presented here is also available through the Zenodo repository, providing an alternative access point in case of difficulties retrieving the single-cruise information from NCEI.

Each XBT file includes the main variables summarized in Table 7, the relative EMODNet-compliant metadata (i.e., about probe type, software, manufacturer, data originator, scientific project, platform, uncertainties, QF code), detailed information about the FRE coefficients used for temperature and depth bias correction described in section 2.3, and a short description of the dataset. The manufacturer

405 FRE coefficients are also provided in the metadata, allowing anyone who wishes to recalculate the  
 406 corrections in a different way than using Cheng et al. (2014).  
 407 One file is created for each research cruise. The naming convention is xbt\_cruise, where cruise is the  
 408 identification “cruise name” of the PNRA research expedition, as in Table 1. Please note that the  
 409 format and labels of the provided XBT text files are ODV-compliant to facilitate ease of use.  
 410 Additionally, a Python code for basic XBT data visualization is included in supplemental material  
 411 S37 (such as shown for scatter plots of vertical temperature profiles and latitudinal temperature  
 412 sections in Figures S38 and S39).

413

414 **Table 6.** XBT data repository list

Data set	DOI	Reference
PNRA_X – 1st leg	<a href="https://doi.org/10.7289/v5rf5s9v">https://doi.org/10.7289/v5rf5s9v</a>	Cotroneo et al., 2018a
PNRA_X – 2nd leg	<a href="https://doi.org/10.7289/v53r0r5z">https://doi.org/10.7289/v53r0r5z</a>	Cotroneo et al., 2018b
PNRA_XI	<a href="https://doi.org/10.7289/v5x065b9">https://doi.org/10.7289/v5x065b9</a>	Cotroneo et al., 2018c
PNRA_XII	<a href="https://doi.org/10.7289/v5kd1w6b">https://doi.org/10.7289/v5kd1w6b</a>	Cotroneo et al., 2018d
PNRA_XIII	<a href="https://doi.org/10.7289/v50863mf">https://doi.org/10.7289/v50863mf</a>	Cotroneo et al., 2018e
PNRA_XIV	<a href="https://doi.org/10.7289/v5mg7mtc">https://doi.org/10.7289/v5mg7mtc</a>	Cotroneo et al., 2018f
PNRA_XV	<a href="https://doi.org/10.7289/v56d5r8p">https://doi.org/10.7289/v56d5r8p</a>	Cotroneo et al., 2018g
PNRA_XVI	<a href="https://doi.org/10.7289/v5s75dpg">https://doi.org/10.7289/v5s75dpg</a>	Cotroneo et al., 2018h
PNRA_XVII	<a href="https://doi.org/10.7289/v5ng4nzt">https://doi.org/10.7289/v5ng4nzt</a>	Cotroneo et al., 2018i
PNRA_XVIII	<a href="https://doi.org/10.7289/v5qz289c">https://doi.org/10.7289/v5qz289c</a>	Cotroneo et al., 2018j
PNRA_XIX	<a href="https://doi.org/10.7289/v5vq3113">https://doi.org/10.7289/v5vq3113</a>	Cotroneo et al., 2018k
PNRA_XX	<a href="https://doi.org/10.7289/v5vh5m45">https://doi.org/10.7289/v5vh5m45</a>	Cotroneo et al., 2018l
PNRA_XXI	<a href="https://dx.doi.org/10.25921/hzcp-d813">https://dx.doi.org/10.25921/hzcp-d813</a>	Cotroneo et al., 2019
PNRA_XXII	<a href="https://doi.org/10.25921/c8bm-xh74">https://doi.org/10.25921/c8bm-xh74</a>	Cotroneo et al., 2018m
PNRA_XXIII	<a href="https://doi.org/10.25921/q29v-c980">https://doi.org/10.25921/q29v-c980</a>	Cotroneo et al., 2018n
PNRA_XXV	<a href="https://doi.org/10.7289/v50r9mmm">https://doi.org/10.7289/v50r9mmm</a>	Cotroneo et al., 2017a
PNRA_XXVII	<a href="https://doi.org/10.7289/v54j0cbw">https://doi.org/10.7289/v54j0cbw</a>	Cotroneo et al., 2017b
PNRA_XXVIII	<a href="https://doi.org/10.25921/9YTS-P771">https://doi.org/10.25921/9YTS-P771</a>	Cotroneo et al., 2018o
PNRA_XXIX	<a href="https://doi.org/10.25921/220j-b370">https://doi.org/10.25921/220j-b370</a>	Cotroneo et al., 2024a
PNRA_XXX	<a href="https://doi.org/10.25921/9ph6-c102">https://doi.org/10.25921/9ph6-c102</a>	Cotroneo et al., 2024b
PNRA_XXXI	<a href="https://doi.org/10.25921/zf04-ch06">https://doi.org/10.25921/zf04-ch06</a>	Cotroneo et al., 2024c
PNRA_XXXII	<a href="https://doi.org/10.25921/vvmp-rr55">https://doi.org/10.25921/vvmp-rr55</a>	Cotroneo et al., 2024d
PNRA_XXXIV	<a href="https://doi.org/10.25921/jeee-zf77">https://doi.org/10.25921/jeee-zf77</a>	Cotroneo et al., 2024e
PNRA_XXXV	<a href="https://doi.org/10.25921/1ysg-dw94">https://doi.org/10.25921/1ysg-dw94</a>	Cotroneo et al., 2024f
PNRA_XXXVI	<a href="https://doi.org/10.25921/aeg5-hw87">https://doi.org/10.25921/aeg5-hw87</a>	Cotroneo et al., 2024g
PNRA_XXXVII	<a href="https://doi.org/10.25921/3mmd-tj60">https://doi.org/10.25921/3mmd-tj60</a>	Cotroneo et al., 2024h
PNRA_XXXVIII	<a href="https://doi.org/10.25921/kte7-d058">https://doi.org/10.25921/kte7-d058</a>	Cotroneo et al., 2024i
PNRA_XXXIX	<a href="https://doi.org/10.25921/jc13-ek97">https://doi.org/10.25921/jc13-ek97</a>	Cotroneo et al., 2024l

415

416 **Table 7.** Name and description of the main variables included in the XBT text files.

Name of variable	Unit	Description
Cruise		Cruise name
Station		Identifier number of XBT deployment
Type		Instrument type
Date	dd/mm/yyyy	Date of XBT deployment
Time	hh:mm	Time of XBT deployment
Latitude [degrees_north]	Decimal degrees	Latitude of XBT deployment
Longitude [degrees_east]	Decimal degrees	Longitude of XBT deployment
Bot. Depth [m]	Meters	Maximum depth reached by the XBT probe
Elapsed Time [s]	Seconds	Time elapsed since the release of the XBT probe
Depth 1 [m]	Meters	Depth derived from the elapsed time using the Manufacturer Fall Rate Equation Coefficients
Depth 2 [m]	Meters	Depth derived from the elapsed time using the Hanawa et al. (1995) Fall Rate Equation Coefficients
Depth 3 [m]	Meters	Depth 2 corrected following Cheng et al. (2014) with Hanawa et al. (1995) Fall Rate Equation Coefficients
Temperature 1 [°C]	Celsius degrees	Temperature measured by the XBT probe
Temperature 2 [°C]	Celsius degrees	Temperature corrected following Cheng et al. (2014) with Hanawa et al. (1995) Fall Rate Equation Coefficients
QF	0 – 4	Quality flags of XBT measurements

417

## 418 **5. Conclusions**

419 The SO is a key place for atmosphere–ocean physical and biogeochemical interactions at different  
 420 spatial and temporal scales (Falco and Zambianchi, 2011; Cerrone et al., 2017a, b; Buongiorno  
 421 Nardelli et al., 2017). However, despite their importance, processes in many areas of the SO are still  
 422 poorly known due to the scarcity of in situ measurements. This is particularly true for the ACC region  
 423 and its fronts, which are characterized by complex dynamics and intense eddy activity (Trani et al.,  
 424 2011; Cotroneo et al., 2013; Frenger et al., 2015, Menna et al., 2020; Ferola et al., 2023). To fill this  
 425 gap, all available measurements provide a significant contribution and should be shared within the  
 426 oceanographic community.

427 To this goal, here we present 36 vertical sections of XBT ocean temperature data collected between  
 428 New Zealand and the Ross Sea (PX36 line) during the Austral summers from 1994/1995 to  
 429 2022/2023. This dataset provides direct insights into the 0-800 m thermal characteristics of the Pacific  
 430 sector of the SO and complements data sourced from observing networks, drifters, ARGO floats and  
 431 glider fleets. It is also suitable to be combined with enhanced spatial and temporal scale remotely  
 432 sensed observations and numerical simulations. This comprehensive dataset lays a robust foundation  
 433 for a nuanced analysis of the key mechanisms governing thermohaline circulation in the SO and for  
 434 improving our knowledge of the physical and biogeochemical characteristics of the four-dimensional  
 435 ocean.

436 The continuation of this XBT collection over time, in the framework of the Italian PNRA research  
437 expeditions to Antarctica, is particularly important due to the inherent challenges associated with data  
438 acquisition in the SO and promises an increasingly comprehensive and detailed understanding of  
439 thermal variations in this specific maritime region.

440

441 **Author contributions.** GA, YC and AIF conceived and designed the manuscript. GA, YC, PC, PF, GF, GB, NK, GS, EZ and  
442 AIF collected the measurements and organized the XBT dataset. GA, YC, LF and AIF carried out the quality control analyses. All  
443 authors analysed the achieved results, contributed to the writing, and approved the final manuscript.

444

445 **Competing interests.** The authors declare that they have no conflict of interest.

446

447 **Acknowledgements.** This study was made possible thanks to the contribution of the Climatic Long-term Interaction for the  
448 Mass balance in Antarctica (CLIMA), Southern Ocean Chokepoints Italian Contribution (SOChIC), Marine Observatory of the Ross  
449 Sea (MORSea), Effects of the east current on the Salinity variability in the Ross Sea (ESTRO), Physical and biogeochemical tracing  
450 of water masses at source areas and export gates in the Ross Sea and impact on the Southern Ocean (SIGNATURE) and Antarctic  
451 Circumpolar Current Eddies Survey and Simulations (ACCESS) projects, part of the Italian National Antarctic Research Program  
452 (PNRA). Special thanks go to Arturo De Alteris, Massimo De Stefano, Massimiliano Esposito and Giovanni Zambardino who provided  
453 essential support to data acquisition, as well as to the captain, officers, and crew of the research vessels used for XBT launches. The  
454 authors are particularly grateful to the ESSD referees and editors for the constructive comments and suggestions provided during the  
455 manuscript discussion.

456

457

## 458 References

459

460 Armour, K.C., Marshall, J., Scott, J.R., Donohoe, A. and Newsom, E.R.: Southern Ocean warming  
461 delayed by circumpolar upwelling and equatorward transport, *Nat. Geosci.*, 9, 549–554,  
462 <https://doi.org/10.1038/ngeo2731>, 2016.

463

464 Aulicino, G. and Wadhams, P.: Editorial for the Special Issue “Remote Sensing of the Polar Oceans”.  
465 *Remote Sens.*, 14, 6195, <https://doi.org/10.3390/rs14246195>, 2022.

466

467 Aulicino, G., Cotroneo, Y., de Ruggiero, P., Buono, A., Corcione, V., Nunziata, F., Fusco, G.: Remote  
468 Sensing Applications in Satellite Oceanography, In P. Daponte et al. (eds.), *Measurement for the Sea*,  
469 Springer Series in Measurement Science and Technology, [http://dx.doi.org/10.1007/978-3-030-](http://dx.doi.org/10.1007/978-3-030-82024-4_8)  
470 [82024-4\\_8](http://dx.doi.org/10.1007/978-3-030-82024-4_8), 2022.

471

472 Aulicino, G., Cotroneo, Y., and Ferola, A. I.: XBT water column temperature data collected in the  
473 Southern Ocean between New Zealand and the Ross Sea during the austral summers from 1994/1995  
474 to 2023/2024 [Data set]. Zenodo, <https://doi.org/10.5281/zenodo.14848849>, 2025.

475

476 Bailey, R., Gronell, A., Phillips, H., Tanner, E., and Meyers, G.: Quality control cookbook for XBT  
477 data, Version 1.1. CSIRO Marine Laboratories Reports, 221, <https://doi.org/10.25607/OBP-1482>,  
478 1994.

479

480 Belkin, I. M. and Gordon, A. L.: Southern Ocean fronts from the Greenwich meridian to Tasmania,  
481 *J. Geophys. Res.*, 101, <https://doi.org/10.1029/95JC02750>, 1996.

482

483 Botnikov, V. N.: Geographical position of the Antarctic Convergence Zone in the Antarctic  
484 Ocean, *Soviet Antarctic Exped. Inform. Bull.*, 41, 324–327, 1963.

485

- Budillon, G. and Rintoul, S. R.: Fronts and upper ocean thermal variability south of New Zealand, *Antartct. Sci.*, 15, 141-152, <https://doi.org/10.1017/S0954102003001135>, 2003.
- Buongiorno Nardelli, B., Guinehut, S., Verbrugge, N., Cotroneo, Y., Zambianchi, E., and Iudicone, D.: Southern Ocean mixed-layer seasonal and interannual variations from combined satellite and in situ data, *J. Geophys. Res.: Oceans*, 122(12), <https://doi.org/10.1002/2017JC013314>, 2017.
- Buongiorno Nardelli, B.: A Deep Learning Network to Retrieve Ocean Hydrographic Profiles from Combined Satellite and In Situ Measurements, *Remote Sens.*, 12, 3151. <https://doi.org/10.3390/rs12193151>, 2020.
- Cerrone, D., Fusco, G., Cotroneo, Y., Simmonds, I., and Budillon, G.: The Antarctic circumpolar wave: Its presence and interdecadal changes during the last 142 years, *J. Climate*, 30(16), 6371–6389, <https://doi.org/10.1175/JCLI-D-16-0646.1>, 2017a.
- Cerrone, D., Fusco, G., Simmonds, I., Aulicino, G., and Budillon, G.: Dominant covarying climate signals in the Southern Ocean and Antarctic sea ice influence during the last three decades. *J. Climate*, 30(8), 3055–3072, <https://doi.org/10.1175/JCLI-D-16-0439.1>, 2017b.
- Chelton, D. B., Schlax, M. G., Samelson, R. M.: Global observations of nonlinear mesoscale eddies, *Prog. Oceanogr.*, Volume 91, Issue 2, 167-216, <https://doi.org/10.1016/j.pocean.2011.01.002>, 2011.
- Chen, Z., Wang, X., Cao, H., Song, X.: Mapping high-resolution surface current by incorporating geostrophic equilibrium with surface quasigeostrophic theory using multi-source satellite observations, *Remote Sens. Environ.*, 304, <https://doi.org/10.1016/j.rse.2024.114058>, 2024.
- Chen, X., Chen, G., Ge, L., Cao, C. and Huang, B.: Medium-range forecasting of oceanic eddy trajectory, *Int. J. Digit. Earth*, 17:1, <https://doi.org/10.1080/17538947.2023.2300325>, 2024.
- Cheng, L., J. Zhu, R. Cowley, T. Boyer, and S. Wijffels: Time, probe type, and temperature variable bias corrections to historical expendable bathythermograph observations. *J. Atmos. Oceanic Technol.*, 31, 1793-1825, <https://doi.org/10.1175/Jtech-D-13-00197.1>, 2014.
- Cheng, L., Abraham, J., Goni, G., Boyer, T., et al.: XBT Science: assessment of instrumental biases and errors, *Bulletin of the American Meteorological Society*, 97, 924-933. <http://dx.doi.org/10.1175/BAMS-D-15-00031>, 2016.
- Convey, P., and Peck, L. S.: Antarctic environmental change and biological responses, *Sci. Adv.*, <https://doi.org/10.1126/sciadv.aaz0888>, 2019.
- Cotroneo, Y., Budillon, G., Fusco, G. and Spezie, G.: Cold core eddies and fronts of the Antarctic Circumpolar Current south of New Zealand from in situ and satellite data, *J. Geophys. Res. Oceans*, 118, 2653–2666, <https://doi.org/10.1002/jgrc.20193>, 2013.
- Cotroneo, Y., Aulicino, G., Ruiz, S., Pascual, A., Budillon, G., Fusco, G., and Tintoré, J.: Glider and satellite high resolution monitoring of a mesoscale eddy in the Algerian basin: Effects on the mixed layer depth and biochemistry, *J. Mar. Syst.*, 162, 73-88, <https://doi.org/10.1016/j.jmarsys.2015.12.004>, 2016.

535 Cotroneo, Y., Budillon, G., Artegiani, A., Conversano, F., Corbo, C., Gallarato, A., et al.: Water  
536 temperature data from XBT taken from the research vessel *Italica* in the Southern Ocean and  
537 Southwest Pacific Ocean from 1994-11-03 to 1995-01-01 (NCEI Accession 0170608), NOAA  
538 National Centers for Environmental Information. <https://doi.org/10.7289/v5rf5s9v>, 2018a.  
539

540 Cotroneo, Y., Budillon, G., Artegiani, A., Conversano, F., Corbo, C., Gallarato, A., et al.: Water  
541 temperature data from XBT taken from the research vessel *Italica* in the Southern Ocean and  
542 Southwest Pacific Ocean from 1995-01-06 to 1995-03-02 (NCEI Accession 0170765), NOAA  
543 National Centers for Environmental Information. <https://doi.org/10.7289/v53r0r5z>, 2018b.  
544

545 Cotroneo, Y., Budillon, G., Artegiani, A., Ferrara, C., Meloni, R., & Spezie, G.: Water temperature  
546 from XBT taken from research vessel *Italica* in the Southern Ocean and Southwest Pacific Ocean  
547 from 1996-01-07 to 1996-02-18 (NCEI Accession 0171481), NOAA National Centers for  
548 Environmental Information. <https://doi.org/10.7289/v5x065b9>, 2018c.  
549

550 Cotroneo, Y., Budillon, G., Conversano, F., Ferrara, C., & Spezie, G.: Water temperature from XBT  
551 taken from the research vessel *Italica* in the Southern Ocean and Southwest Pacific Ocean from 1997-  
552 01-26 to 1997-02-19 (NCEI Accession 0172042), NOAA National Centers for Environmental  
553 Information. <https://doi.org/10.7289/v5kd1w6b>, 2018d.  
554

555 Cotroneo, Y., Budillon, G., Bergamasco, A., Capello, M., De Stefano, M., Ferrara, C., et al.: Water  
556 temperature data from XBT collected from research vessel *Italica* in Southern Ocean and Southwest  
557 Pacific Ocean from 1997-11-23 to 1998-03-06 (NCEI Accession 0172859). NOAA National Centers  
558 for Environmental Information. <https://doi.org/10.7289/v50863mf>, 2018e.  
559

560 Cotroneo, Y., Budillon, G., Ferrara, C., Meloni, R., Paschini, E., & Spezie, G.: Water temperature  
561 from XBT taken from the research vessel *Italica* in the Southern Ocean and Southwest Pacific Ocean  
562 from 1999-01-05 to 1999-01-11 (NCEI Accession 0173211), NOAA National Centers for  
563 Environmental Information. <https://doi.org/10.7289/v5mg7mtc>, 2018f.  
564

565 Cotroneo, Y., Budillon, G., Ferrara, C., Paschini, E., Russo, A., & Spezie, G.: Water temperature from  
566 XBT taken from the research vessel *Italica* in the Southern Ocean and Southwest Pacific Ocean from  
567 2000-01-07 to 2000-02-18 (NCEI Accession 0173212), NOAA National Centers for Environmental  
568 Information. <https://doi.org/10.7289/v56d5r8p>, 2018g.  
569

570 Cotroneo, Y., Budillon, G., Bergamasco, A., De Stefano, M., Ferrara, C., Paschini, E., & Spezie, G.:  
571 Water temperature from XBT taken from the research vessel *Italica* in the Southern Ocean and  
572 Southwest Pacific Ocean from 2001-01-06 to 2001-02-26 (NCEI Accession 0173213), NOAA  
573 National Centers for Environmental Information. <https://doi.org/10.7289/v5s75dpg>, 2018h.  
574

575 Cotroneo, Y., Budillon, G., Ferrara, C., Orsi, M., Paschini, E., Rivaro, P., & Spezie, G.: Water  
576 temperature from XBT taken from the research vessel *Italica* in the Southern Ocean and Southwest  
577 Pacific Ocean from 2001-12-24 to 2001-12-31 (NCEI Accession 0173214), NOAA National Centers  
578 for Environmental Information. <https://doi.org/10.7289/v5ng4nzt>, 2018i.  
579

580 Cotroneo, Y., Budillon, G., Bergamasco, A., De Alteris, A., De Stefano, M., Ferrara, C., et al.: Water  
 581 temperature from XBT taken from the research vessel *Italica* in the Southern Ocean and Southwest  
 582 Pacific Ocean from 2003-01-06 to 2003-01-11 (NCEI Accession 0173338), NOAA National Centers  
 583 for Environmental Information. <https://doi.org/10.7289/v5qz289c>, 2018j.

584

585 Cotroneo, Y., Budillon, G., Ferrara, C., Monteduro, R., Russo, A., & Spezie, G.: Water temperature  
 586 from XBT taken from the research vessel *Italica* in the Southern Ocean and Southwest Pacific Ocean  
 587 from 2003-12-24 to 2003-12-28 (NCEI Accession 0173328), NOAA National Centers for  
 588 Environmental Information. <https://doi.org/10.7289/v5vq3113>, 2018k.

589

590 Cotroneo, Y., Budillon, G., Aliani, S., Capello, M., Ferrara, C., Paschini, E. & Spezie, G.: Water  
 591 temperature from XBT taken from the research vessel *Italica* in the Southern Ocean and Southwest  
 592 Pacific Ocean from 2005-01-01 to 2005-01-06 (NCEI Accession 0173533), NOAA National Centers  
 593 for Environmental Information. <https://doi.org/10.7289/v5vh5m45>, 2018l.

594

595 Cotroneo, Y., Budillon, G., Ferrara, C., Meloni, R., & Spezie, G.: Water temperature from XBT taken  
 596 from the research vessel *Italica* in the Southern Ocean and Southwest Pacific Ocean from 2007-02-  
 597 05 to 2007-02-10 (NCEI Accession 0174709). Version 1.1, NOAA National Centers for  
 598 Environmental Information. <https://doi.org/10.25921/c8bm-xh74>, 2018m.

599

600 Cotroneo, Y., Budillon, G., Aliani, S., Ferrara, C., Greco, A., Meloni, R. & Spezie, G.: Water  
 601 temperature from XBT taken from the research vessel *Italica* in the Southern Ocean and Southwest  
 602 Pacific Ocean from 2008-01-16 to 2008-01-21 (NCEI Accession 0174711), Version 1.1. NOAA  
 603 National Centers for Environmental Information. <https://doi.org/10.25921/q29v-c980>, 2018n.

604

605 Cotroneo, Y., Budillon, G., Meloni, R., Aliani, S., Zambardino, G., & Spezie, G.: Water temperature  
 606 data from XBT taken from research vessel *Italica* in the Southern Ocean and Southwest Pacific Ocean  
 607 from 2010-01-25 to 2010-01-29 (NCEI Accession 0167835), NOAA National Centers for  
 608 Environmental Information. <https://doi.org/10.7289/v50r9mmm>, 2017a.

609

610 Cotroneo, Y., Budillon, G., Castagno, P., De Alteris, A., De Stefano, M., Falco, P., et al.: Water  
 611 temperature from XBT taken from research vessel *Italica* in the Southern Ocean and Southwest  
 612 Pacific Ocean from 2012-01-13 to 2012-01-19 (NCEI Accession 0167834). NOAA National Centers  
 613 for Environmental Information. <https://doi.org/10.7289/v54j0cbw>, 2017b.

614

615 Cotroneo, Y., Budillon, G., Castagno, P., Colizza, E., Cotterle, D., Falco, P., et al.: Water temperature  
 616 from XBT taken from the research vessel *Araon* in the Southern Ocean and Southwest Pacific Ocean  
 617 from 2013-01-24 to 2013-02-06 (NCEI Accession 0174794). Version 1.1, NOAA National Centers  
 618 for Environmental Information. <https://doi.org/10.25921/9YTS-P771>, 2018o.

619

620 Cotroneo, Y., Budillon, G., Falco, P., Fusco, G., et al.: Water temperature from XBT taken from the  
 621 research vessel *Italica* in the Southern Ocean and Southwest Pacific Ocean from 2006-01-01 to 2006-  
 622 01-04 (NCEI Accession 0207044). NOAA National Centers for Environmental Information.  
 623 <https://doi.org/10.25921/hzcp-d813>, 2019.

624

625 Cotroneo, Y., Ferola, A.I., Aulicino, G., Castagno, P. et al.: Water temperature taken by XBT from  
626 the research vessel *Italica* in the Southern Ocean (> 60 degrees South) and Southwest Pacific Ocean  
627 (limit-147 E to 140 W) from 2013-12-30 to 2014-02-18 (NCEI Accession 0287161). NOAA National  
628 Centers for Environmental Information. <https://doi.org/10.25921/220j-b370>, 2024a.

629

630 Cotroneo, Y., Ferola, A.I., Aulicino, G., Castagno, P. et al.: Water temperature taken by XBT from  
631 the research vessel *Araon* in the Southern Ocean (> 60 degrees South) and Southwest Pacific Ocean  
632 (limit-147 E to 140 W) from 2015-01-02 to 2015-01-10 (NCEI Accession 0287162). NOAA National  
633 Centers for Environmental Information. <https://doi.org/10.25921/9ph6-c102>, 2024b.

634

635 Cotroneo, Y., Ferola, A.I., Aulicino, G., Castagno, P. et al.: Water temperature taken by XBT from  
636 the research vessel *Italica* in the Southern Ocean (> 60 degrees South) and Southwest Pacific Ocean  
637 (limit-147 E to 140 W) from 2016-01-16 to 2016-01-28 (NCEI Accession 0287159). NOAA National  
638 Centers for Environmental Information. <https://doi.org/10.25921/zf04-ch06>, 2024c.

639

640 Cotroneo, Y., Ferola, A.I., Aulicino, G., Castagno, P. et al.: Water temperature taken by XBT from  
641 the research vessel *Italica* in the Southern Ocean (> 60 degrees South) and Southwest Pacific Ocean  
642 (limit-147 E to 140 W) from 2016-12-31 to 2017-01-05 (NCEI Accession 0287163). NOAA National  
643 Centers for Environmental Information. <https://doi.org/10.25921/vvmp-rr55>, 2024d.

644

645 Cotroneo, Y., Ferola, A.I., Aulicino, G., Castagno, P. et al.: Water temperature taken by XBT from  
646 the research vessel *Araon* in Southern Oceans (> 60 degrees South) and Southwest Pacific Ocean  
647 (limit-147 E to 140 W) from 2019-02-08 to 2019-02-12 (NCEI Accession 0287554). NOAA National  
648 Centers for Environmental Information. <https://doi.org/10.25921/jeee-zf77>, 2024e.

649

650 Cotroneo, Y., Ferola, A.I., Aulicino, G., Castagno, P. et al.: Water temperature taken by XBT from  
651 the research vessel *Laura Bassi* in the Southern Ocean (> 60 degrees South) and Southwest Pacific  
652 Ocean (limit-147 E to 140 W) from 2020-01-07 to 2020-01-12 (NCEI Accession 0287549). NOAA  
653 National Centers for Environmental Information. <https://doi.org/10.25921/1ysg-dw94>, 2024f.

654

655 Cotroneo, Y., Ferola, A.I., Aulicino, G., Castagno, P. et al.: Water temperature taken by XBT from  
656 the research vessel *Laura Bassi* in the Southern Ocean (> 60 degrees South) and Southwest Pacific  
657 Ocean (limit-147 E to 140 W) from 2020-12-25 to 2021-01-02 (NCEI Accession 0297164). NOAA  
658 National Centers for Environmental Information. <https://doi.org/10.25921/aeg5-hw87>, 2024g.

659

660 Cotroneo, Y., Ferola, A.I., Aulicino, G., Castagno, P. et al.: Water temperature taken by XBT from  
661 the research vessel *Laura Bassi* in the Southern Ocean (> 60 degrees South) and Southwest Pacific  
662 Ocean (limit-147 E to 140 W) from 2022-01-08 to 2022-01-26 (NCEI Accession 0297165). NOAA  
663 National Centers for Environmental Information. <https://doi.org/10.25921/3mmd-tj60>, 2024h.

664

665 Cotroneo, Y., Ferola, A.I., Aulicino, G., Castagno, P. et al.: Water temperature taken by XBT from  
666 the research vessel *Laura Bassi* in the Southern Ocean (> 60 degrees South) and Southwest Pacific  
667 Ocean (limit-147 E to 140 W) from 2023-01-06 to 2023-01-12 (NCEI Accession 0297163). NOAA  
668 National Centers for Environmental Information. <https://doi.org/10.25921/kte7-d058>, 2024i.

669



670 Cotroneo, Y., Ferola, A.I., Aulicino, G., Castagno, P. et al.: Water temperature taken by XBT from  
671 the research vessel Laura Bassi in the Southern Ocean (> 60 degrees South) and Southwest Pacific  
672 Ocean (limit-147 E to 140 W) from 2024-01-07 to 2024-01-12 (NCEI Accession 0297166). NOAA  
673 National Centers for Environmental Information. <https://doi.org/10.25921/jc13-ek97>, 2024l.

674

675 Cowley, R., Wijffels, S., Cheng, L., Boyer, T. and Kizu, S.: Biases in expendable bathythermograph  
676 data: A new view based on historical side-by-side comparisons. *J. Atmos. Oceanic Technol.*, 30,  
677 1195–1225, <https://doi.org/10.1175/JTECH-D-12-00127.1>, 2013.

678

679 Cowley, R. and Krummel, L. Australian XBT Quality Control Cookbook Version 2.1 (updated  
680 August 2023). CSIRO, Australia. <https://doi.org/10.25919/3tm5-zn80>, 2022.

681

682 Daneshzadeh, Y.H., Festa, J.F. and Minton, S.M.: Procedures used at AOML to quality control real  
683 time XBT data collected in the Atlantic Ocean. Miami, USA, NOAA Atlantic Oceanographic and  
684 Meteorological Laboratory, 44pp, <https://doi.org/10.25607/OBP-1485>, 1994.

685

686 Downes, S.M., Farneti, R., Uotila, P., Griffies, S.M., Marsland, S.J. et al.: An assessment of Southern  
687 Ocean water masses and sea ice during 1988–2007 in a suite of interannual CORE-II simulations,  
688 *Ocean Model.*, 94, 67-94, <https://doi.org/10.1016/j.ocemod.2015.07.022>, 2015.

689

690 Falco, P. and Zambianchi, E.: Near-surface structure of the Antarctic Circumpolar Current derived  
691 from World Ocean Circulation Experiment drifter data, *J. Geophys. Res. Oceans*, 116(C5),  
692 <https://doi.org/10.1029/2010JC006349>, 2011.

693

694 Falco, P., Castagno, P., Cotroneo, Y., Aulicino, G., Budillon, G., de Ruggiero, P., Fusco, G. and  
695 Zambianchi, G.: Measurements for Oceanography. In P. Daponte et al. (eds.), *Measurement for the*  
696 *Sea*, Springer Series in Measurement Science and Technology, [http://dx.doi.org/10.1007/978-3-030-](http://dx.doi.org/10.1007/978-3-030-82024-4_3)  
697 [82024-4\\_3](http://dx.doi.org/10.1007/978-3-030-82024-4_3), 2022.

698

699 Ferola, A. I., Cotroneo, Y., Wadhams, P., Fusco, G., Falco, P., Budillon, G., and Aulicino, G.: The  
700 Role of the Pacific-Antarctic Ridge in Establishing the Northward Extent of Antarctic Sea-Ice,  
701 *Geophys. Res. Lett.*, 50(10), <https://doi.org/10.1029/2023GL104373>, 2023.

702

703 Frenger, I., Münnich, M., Gruber, N., and Knutti, R.: Southern Ocean eddy phenomenology, *J.*  
704 *Geophys. Res. Oceans*, 120, 7413–7449, <https://doi.org/10.1002/2015JC011047>, 2015.

705

706 GEBCO Compilation Group: GEBCO 2023 Grid, [https://doi.org/10.5285/f98b053b-0cbc-6c23-](https://doi.org/10.5285/f98b053b-0cbc-6c23-e053-6c86abc0af7b)  
707 [e053-6c86abc0af7b](https://doi.org/10.5285/f98b053b-0cbc-6c23-e053-6c86abc0af7b), 2023.

708

709 Gille, S. T.: Mean sea surface height of the Antarctic Circumpolar Current from GEOSAT 600 data:  
710 methods and application, *J. Geophys. Res.*, 99, 18255-18273, <https://doi.org/10.1029/94JC01172>,  
711 1994.

712

713 Goni, G., and coauthors: More than 50 years of successful continuous temperature section  
714 measurements by 943 the global expendable bathythermograph network, its integrability, societal  
715 benefits, and future. *Front. Mar. Sci.*, 6:452, <https://doi.org/10.3389/fmars.2019.00452>, 2019.

716

717 Gouretski, V. and Reseghetti, F.: On depth and temperature biases in bathythermograph data:  
718 Development of a new correction scheme based on analysis of a global ocean database. *Deep-Sea*  
719 *Res. I*, 57, 812–833, <https://doi.org/10.1016/j.dsr.2010.03.011>, 2010.

720  
721 Green, A. W.: Bulk dynamics of the expendable bathythermograph (XBT). *Deep-Sea Res.*, 31A, 415–  
722 426, [https://doi.org/10.1016/0198-0149\(84\)90093-1](https://doi.org/10.1016/0198-0149(84)90093-1), 1984.  
723  
724 Hanawa, K., Rual, P., Bailey, R., Sy, A., and Szabados, M.: A new depth-time equation for Sippican  
725 or TSK T-7, T-6 and T-4 expendable bathythermographs (XBT), *Deep-Sea Res. I*, 42(8), 1423-1451,  
726 [https://doi.org/10.1016/0967-0637\(95\)97154-Z](https://doi.org/10.1016/0967-0637(95)97154-Z), 1995.  
727  
728 Intergovernmental Oceanographic Commission (2013) *Ocean Data Standards Volume 3.*  
729 *Recommendation for a Quality Flag Scheme for the Exchange of Oceanographic and Marine*  
730 *Meteorological Data.* Paris, France, UNESCO-IOC, 5pp. & Annexes. Intergovernmental  
731 Oceanographic Commission Manuals and Guides, Vol. 54(3). <http://dx.doi.org/10.25607/OBP-6>.  
732  
733 Legler, D.M., Freeland, H.J., Lumpkin, R., Ball, G., McPhaden, M.J., North, S., Crowley, R., Goni,  
734 G.J., Send, U., and Merrifield, M.A.: The current status of the real-time in situ Global Ocean  
735 Observing System for operational oceanography, *J. Oper. Oceanogr.*, 8:sup2, s189-s200,  
736 <https://doi.org/10.1080/1755876X.2015.1049883>, 2015.  
737  
738 McGillicuddy Jr, D. J.: Mechanisms of physical-biological-biogeochemical interaction at the oceanic  
739 mesoscale, *Ann. Rev. Mar. Sci.*, 8, 125-159, [https://doi.org/10.1146/annurev-marine-010814-](https://doi.org/10.1146/annurev-marine-010814-015606)  
740 [015606](https://doi.org/10.1146/annurev-marine-010814-015606), 2016.  
741  
742 Menna, M., Cotroneo, Y., Falco, P., Zambianchi, E., Di Lemma, R., Poulain, P. M. and Budillon, G.:  
743 Response of the Pacific Sector of the Southern Ocean to wind stress variability from 1995 to 2017, *J.*  
744 *Geophys. Res. Oceans*, 125(10), <https://doi.org/10.1029/2019JC015696>, 2020.  
745  
746 Morales Maqueda, M. A., Willmott, A. J. and Biggs, N. R. T.: Polynya dynamics: A review of  
747 observations and modelling, *Rev. Geophys.*, 42.1, <https://doi.org/10.1029/2002RG000116>, 2004.  
748  
749 Orsi, A. H., Whitworth, T., and Nowlin, W. D.: On the meridional extent and fronts of the Antarctic  
750 circumpolar current, *Deep-Sea Res. I*, 42(5), 641–673, [https://doi.org/10.1016/0967-0637\(95\)00021-](https://doi.org/10.1016/0967-0637(95)00021-W)  
751 [W](https://doi.org/10.1016/0967-0637(95)00021-W), 1995.  
752  
753 Parks, J., Bringas, F., Cowley, R., Hanstein, C., Krummel, L., Sprintall, J., Cheng, L., Cirano, M.,  
754 Cruz, S., Goes, M., Kizu, S. and Reseghetti, F.: XBT operational best practices for quality assurance,  
755 *Front. Mar. Sci.*, 9, 991760, <https://doi.org/10.3389/fmars.2022.991760>, 2022  
756  
757 Reverdin, G., Marin, F. Bourles, B. and L’Herminier, P.: XBT temperature errors during French  
758 research cruises (1999–2007). *J. Atmos. Oceanic Technol.*, 26, 2462–2473,  
759 <https://doi.org/10.1175/2009JTECHO655.1>, 2009.  
760  
761 Rintoul, S. R., Donguy, J. R., and Roemmich, D. H.: Seasonal evolution of upper ocean thermal  
762 structure between Tasmania and Antarctica. *Deep-Sea Res. I*, 44(7), 1185-1202,  
763 [https://doi.org/10.1016/S0967-0637\(96\)00125-2](https://doi.org/10.1016/S0967-0637(96)00125-2), 1997.  
764  
765 Rintoul, S. R.: The global influence of localized dynamics in the Southern Ocean, *Nature*, 558, 209–  
766 218, <https://doi.org/10.1038/s41586-018-0182-3>, 2018.  
767  
768 Roemmich, D., Wilson, W.S., Gould, W.J., Owens, W.B., Le Traon, P.-Y., Freeland, H.J., King,  
769 B.A., Wijffels, S., Sutton, P.J.H., Zilberman, N.: Chapter 4 - The Argo Program, In *Science of*

770 Sustainable Systems, Partnerships in Marine Research, Auad, G. and Wiese F.K. (eds), Elsevier, 53-  
771 69, <https://doi.org/10.1016/B978-0-323-90427-8.00004-6>, 2022.

772

773 Schlitzer, R. Ocean Data View, <http://odv.awi.de>, 2011.

774

775 Seaver, G.A. and Kuleshov, S.: Experimental and analytical error of the expendable  
776 bathythermograph. *J. Phys. Oceanogr.*, 12, 592–600, [https://doi.org/10.1175/1520-0485\(1982\)012<0592:EAAEOT.2.0.CO;2](https://doi.org/10.1175/1520-0485(1982)012<0592:EAAEOT.2.0.CO;2), 1982.

777

778

779 Seo, H., O'Neill, L. W., Bourassa, M. A., Czaja, A., Drushka, K., Edson, J. B., Fox-Kemper, B.,  
780 Frenger, I., Gille, S. T., Kirtman, B. P., Minobe, S., Pendergrass, A. G., Renault, L., Roberts, M. J.,  
781 Schneider, N., Small, R. J., Stoffelen, A., and Wang, Q.: Ocean Mesoscale and Frontal-Scale Ocean–  
782 Atmosphere Interactions and Influence on Large-Scale Climate: A Review, *J. Climate*, 36(7), 1981–  
783 2013. <https://doi.org/10.1175/JCLI-D-21-0982.1>, 2023.

784

785 Simoncelli, S., Reseghetti, F., Fratianni, C., Cheng, L., and Raiteri, G.: Reprocessing of XBT profiles  
786 from the Ligurian and Tyrrhenian seas over the time period 1999–2019 with full metadata upgrade,  
787 *Earth Syst. Sci. Data Discuss.*, <https://doi.org/10.5194/essd-2023-525>, in review, 2024.

788

789 Sokolov, S. and Rintoul, S. R.: Circulation structure and distribution of the Antarctic circumpolar  
790 current fronts: 2. Variability and relationship to sea surface height, *J. Geophys. Res.*, 114(C11),  
791 C11019, <https://doi.org/10.1029/2008JC005248>, 2009b.

792

793 Sokolov, S. and Rintoul, S. R.: Circumpolar structure and distribution of the Antarctic Circumpolar  
794 Current fronts: 1. Mean circumpolar paths, *J. Geophys. Res.*, 114(C11), C11018,  
795 <https://doi.org/10.1029/2008jc005108>, 2009a.

796

797 Sokolov, S. and Rintoul, S. R.: Multiple Jets of the Antarctic Circumpolar Current South of Australia,  
798 *J. Geophys. Res.*, 37, <https://doi.org/10.1175/JPO3111.1>, 2007.

799

800 Tan, Z., Cheng, L., Gouretski, V., Zhang, B., Wang, Y., Li, F. and Zhu, J.: A new automatic quality  
801 control system for ocean profile observations and impact on ocean warming estimate, *Deep-Sea Res.*  
802 I, 194, 103961, <https://doi.org/10.1016/j.dsr.2022.103961>, 2023.

803

804 Trani, M., Falco, P. and Zambianchi, E.: Near-surface eddy dynamics in the Southern Ocean, *Polar*  
805 *Research*, 30(1), 11203. <https://doi.org/10.3402/polar.v30i0.11203>, 2011.

806

807 Trani, M., Falco, P., Zambianchi, E., and Saltee, J. B.: Aspects of the Antarctic Circumpolar Current  
808 dynamics investigated with drifter data, *Prog. Oceanogr.*, 125, 1–15,  
809 <https://doi.org/10.1016/j.pocean.2014.05.001>, 2014.

810